33. Wood KM, Roff M, Hay RT. Defective IkappaBalpha in Hodgkin cell lines with constitutively active NF-kappaB. Oncogene. 1998;16:2131-2139.

34. Mori N, Fujii M, Ikeda S, et al. Constitutive activation of NF-kappaB in primary adult T-cell leukemia cells. Blood. 1999;93:2360-2368.

35. Yemelyanov A, Gasparian A, Lindholm P, et al. Effects of IKK inhibitor PS1145 on NF-kappaB function, proliferation, apoptosis and invasion activity in prostate carcinoma cells. Oncogene. 2006;25:387-398.

36. Farina AR, Tacconelli A, Vacca A, Maroder M, Gulino A, Mackay AR. Transcriptional up-regulation of matrix metalloproteinase-9 expression during spontaneous epithelial to neuroblast phenotype conversion by SK-N-SH neuroblastoma cells, involved in enhanced invasivity, depends upon GT-box and nuclear factor kappaB elements. Cell Growth Differ. 1999;10:353-367.

37. Collins T, Read MA, Neish AS, Whitley MZ, Thanos D, Maniatis T. Transcriptional regulation of endothelial cell adhesion molecules: NF-kappa B and cytokine-inducible enhancers. FASEB J. 1995;9:899-909.

38. El-Sabban ME, Merhi RA, Haidar HA, et al. Human T-cell lymphotropic virus type 1-transformed cells induce angiogenesis and establish functional gap junctions with endothelial cells. Blood. 2002;99:3383-3389.

39. Mori N, Sato H, Hayashibara T, et al. Human T-cell leukemia virus type I Tax transactivates the matrix metalloproteinase-9 gene: potential role in mediating adult T-cell leukemia invasiveness. Blood. 2002;99:1341-1349.

40. Hayashibara T, Yamada Y, Onimaru Y, et al. Matrix metalloproteinase-9 and

vascular endothelial growth factor: a possible link in adult T-cell leukaemia cell invasion. Br J Haematol. 2002;116:94-102.

41. Fukudome K, Furuse M, Fukuhara N, Orita T, Hinuma Y. Strong induction of ICAM-1 in human T cells transformed by human T-cell leukemia virus type 1 and depression of ICAM-1 or LFA-1 in adult T-cell leukemia-derived cell lines. Int J Cancer. 1992;52:418-427.

42. Mori N, Yamada Y, Ikeda S, et al. Bay 11-7082 inhibits transcription factor NF-kappaB and induces apoptosis of HTLV-I-infected T-cell lines and primary adult T-cell leukemia cells. Blood. 2002;100:1828-1834.

43. Bargou RC, Emmerich F, Krappmann D, et al. Constitutive nuclear factor-kappaB-RelA activation is required for proliferation and survival of Hodgkin's disease tumor cells. J Clin Invest. 1997;100:2961-2969.

44. Yang J, Amiri KI, Burke JR, Schmid JA, Richmond A. BMS-345541 targets inhibitor of kappaB kinase and induces apoptosis in melanoma: involvement of nuclear factor kappaB and mitochondria pathways. Clin Cancer Res. 2006;12:950-960.

45. Gasparian AV, Yao YJ, Kowalczyk D, et al. The role of IKK in constitutive activation of NF-kappaB transcription factor in prostate carcinoma cells. J Cell Sci. 2002;115:141-151.

46. Wang CY, Cusack JC Jr, Liu R, Baldwin AS Jr. Control of inducible chemoresistance: enhanced anti-tumor therapy through increased apoptosis by inhibition of NF-kappaB. Nat Med. 1999;5:412-417.

47. Gilmore TD, Herscovitch M. Inhibitors of NF-kappaB signaling: 785 and counting.

Oncogene. 2006;25:6887-6899.

48. Braun T, Carvalho G, Fabre C, Grosjean J, Fenaux P, Kroemer G. Targeting NF-kappaB in hematologic malignancies. Cell Death Differ. 2006;13:748-758.

49. Courtois G, Gilmore TD. Mutations in the NF-kappaB signaling pathway: implications for human disease. Oncogene. 2006;25:6831-6843.

50. Sun SC, Yamaoka S. Activation of NF-kappaB by HTLV-I and implications for cell transformation. Oncogene. 2005;24:5952-5964.

51. Liptay S, Schmid RM, Nabel EG, Nabel GJ. Transcriptional regulation of NF-kappa B2: evidence for kappa B-mediated positive and negative autoregulation. Mol Cell Biol. 1994;14:7695-7703.

52. Bren GD, Solan NJ, Miyoshi H, Pennington KN, Pobst LJ, Paya CV. Transcription of the RelB gene is regulated by NF-kappaB. Oncogene. 2001;20:7722-7733.

Table 1. Efficiency of colony formation in soft agar

Cells †	Colony-forming efficiency (%)	Average size of colonies (μm) ‡
B5-EV1	0.7 ± 0.5	62.6 ± 1.5
B5-NIK#1	23.2 ± 2.0 *	236.2 ± 12.6 *
B5-NIK#2	18.9 ± 2.4 *	184.1 ± 19.8 *
B5-kd-NIK#1	1.5 ± 0.3	63.1 ± 1.4
B5-kd-NIK#2	1.3 ± 0.1	62.8 ± 1.8
h12-EV1	1.2 ± 0.3	60.5 ± 0.0
h12-NIK#1	12.8 ± 1.7 *	146.9 ± 4.6 *
h12-NIK#2	17.7 ± 1.7 *	154.9 ± 5.6 *
h12-kd-NIK#1	1.4 ± 1.0	61.5 ± 2.1
h12-kd-NIK#2	1.5 ± 0.4	62.5 ± 4.7
B5-EV1-EV2	1.2 ± 0.3	61.8 ± 1.1
B5-NIK#1-EV2	21.1 ± 1.0 *	193.8 ± 3.7 *
B5-NIK#2-EV2	14.3 ± 1.0 *	150.4 ± 8.7 *
h12-EV1-EV2	1.5 ± 0.7	60.8 ± 0.4
h12-NIK#1-EV2	12.3 ± 1.7 *	119.4 ± 5.6 *
h12-NIK#2-EV2	14.0 ± 1.8 *	160.3 ± 7.2 *
B5-EV1-SR-IκBα	1.5 ± 0.0	61.7 ± 0.5
B5-NIK#1-SR-IκBα	3.4 ± 0.0	64.8 ± 1.1
B5-NIK#2-SR-IκBα	3.9 ± 0.1	63.3 ± 0.4
h12-EV1-SR-IκBα	1.7 ± 1.0	61.3 ± 0.4
h12-NIK#1-SR-IκBα	2.7 ± 0.3	62.3 ± 0.1
h12-NIK#2-SR-IκBα	3.4 ± 1.4	61.4 ± 0.2

* $P < .05$ versus B5-EV1.

† Cells were inoculated in 0.33% soft agar and cultured for 3 weeks.

‡ Colonies larger than 60 μm were counted as positive. The sizes of more than 100 positive colonies were averaged.

kd-NIK indicates catalytically inactive NIK; SR, super-repressor; EV1, Empty vector for NIK or kd-NIK; EV2, Empty vector for SR-IκBα.

Legends to the figures

Figure 1. NIK protein is overexpressed in established ATL and Hodgkin Reed-Sternberg cells. (A) Steady state levels of NIK expression in the ATL and H-RS cell lines were revealed by immunoprecipitation-coupled immunoblotting. Approximately 2×10^7 cells were lysed with buffer A. After preclearing, immunoprecipitation was performed at 4°C, using anti-NIK antibody (NIK) or its isotype IgG (IgG). After 3 washes with TNT buffer, immune-complexes were analyzed by immunoblotting with anti-NIK antibody. (B) 293T cells were transfected with pMRX-HA-iresPuro or pMRX-HA-NIKiresPuro for 24 hours. Whole-cell lysates were used as negative and positive controls. ED40515(-) cells were pretreated with (+) or without (-) MG132 (20 μM) for 3 hours, lysed with RIPA buffer and subjected to immunoblotting with anti-NIK or anti-α-tubulin antibodies. Immunoprecipitation-coupled immunoblotting was performed as in (A). (C) Upper panels: control T-cell lines (CEM and Jurkat), leukemic cell lines derived from ATL patients which do not express Tax (ED40515(-), ATL43-Tb(-) and TL-Om1), a control B-cell line (RG69) and H-RS cell lines (HDLM-2 and L540) were pretreated with (+) or without (-) MG132 (20 μM) for 3 hours and 30 μg of the whole-cell extracts were subjected to western blot analysis with the antibodies to the indicated proteins. Lower panels: Whole-cell extracts from the indicated cell lines were analyzed by western blotting with the antibodies to the indicated proteins. (D) Total RNA was extracted from the indicated cell lines and subjected to real-time RT-PCR to quantify the *nik* mRNA levels. The *nik* mRNA levels were normalized to 18S RNA. The relative *nik*

mRNA levels shown represent the fold increases in mRNA abundance, relative to that of the CEM cells (arbitrarily set at 1). (E) Cells were cultured in the presence of actinomycin D (5 μg/ml) for the times indicated, and then total RNA was isolated and subjected to quantitative RT-PCR as in (D). Data are expressed as mean ± SD of three independent experiments. The relative amounts of *nik* mRNA shown represent the percentages in mRNA abundance, relative to that of each cell line before the addition of actinomycin D (arbitrarily set at 100%). Abbreviations used: IB; Immunoblotting, IP; Immunoprecipitation.

Figure 2. Overexpression of the *nik* mRNA and protein in PBMCs from ATL patients. (A) Total RNA was extracted from PBMCs from healthy donors and ATL patients, and then subjected to quantitative RT-PCR. The *nik* mRNA levels were normalized to 18S RNA. The relative *nik* mRNA levels shown represent the fold increases in mRNA abundance relative to that of healthy donor 1 (arbitrarily set at 1). These data are expressed as the mean ± SD of three independent experiments. (B) PBMCs were cultured in the presence of actinomycin D (5 μg/ml) for the times indicated, and then total RNA was isolated and subjected to quantitative RT-PCR. The relative amounts of *nik* mRNA shown represent the percentages in mRNA abundance, relative to that of PBMCs before the addition of actinomycin D (arbitrarily set at 100%). (C) PBMCs from a healthy donor and an ATL patient were treated with (+) or without (-) MG132 (20 μM) for 3 hours, lysed with RIPA buffer and subjected to immunoblotting with anti-NIK or anti-α-tubulin antibodies.

Figure 3. NIK induces constitutive NF-κB activity in rat fibroblasts. (A) B5 and h12 cells were infected with retroviruses capable of expressing HA-tagged NIK (NIK) or catalytically inactive NIK (kd-NIK). Pools of B5 and h12 cells transduced with the control pMRX-HAiresPuro vector (EV1) were used as a control. Cytoplasmic extracts from EV1 and two independent cell clones (#1 and #2) were subjected to immunoprecipitation using antibody against the HA epitope. Immunoprecipitates were then resolved by 8% SDS-PAGE and subjected to immunoblotting with anti-NIK antibody. 293T cells were transiently transfected with the pMRX-HAiresPuro vector (EV1) or pMRX-HA-NIKiresPuro (NIK). Cytoplasmic extracts (30 μg) were then used for immunoblotting as negative and positive controls, respectively. (B) Elevated p52 production in rat fibroblasts. Whole-cell lysates from B5 and h12 cells expressing wild type NIK or kd-NIK were subjected to SDS-PAGE and immunoblotting with anti-p52 for detection of p100 and p52 or anti-actin antibodies. (C) Elevated NF-κB DNA binding activity in rat fibroblasts. Five micrograms of nuclear extracts prepared from B5 and h12 cells expressing wild type NIK or kd-NIK were analyzed by EMSA, using oligonucleotides encoding an NF-κB-binding sequence or Oct-1-binding sequence as probes. (D) DNA-binding NF-κB components in B5 and h12 cells expressing wild type NIK were analyzed by super-shift EMSA. Nuclear extracts (5 μg) from B5 NIK#1 and h12 NIK#2 cells were pre-incubated for 30 minutes with pre-immune (PI), anti-p50, anti-RelA or anti-RelB sera, and then subjected to EMSA with the NF-κB-specific probe. Abbreviations used: IB; Immunoblotting, IP; Immunoprecipitation.

Figure 4. NIK expression parallels IKK activity following CHX or MG132 treatment. B5 cells transduced with the control vector (EV1) or B5 cells expressing wild type NIK (NIK#1) were treated for 4 hours with either vehicle (ethanol, EtOH), cycloheximide (CHX; 50 μg/ml) or MG132 (20 μM). Cytoplasmic extracts were subjected to immunoprecipitation with IKK1-specific antibody, and then immunoprecipitates were used for an in vitro kinase assay. IKK1 expression in the immunoprecipitates was revealed by immunoblotting with IKK1-specific antibody. NIK and actin levels in the cytoplasmic extracts used for immunoprecipitation were determined by immunoblotting with anti-NIK or anti-actin antibodies, respectively. Abbreviations used: IB; Immunoblotting, IP; Immunoprecipitation, GST; glutathione-S-transferase tag.

Figure 5. The overexpression of NIK transforms rat fibroblasts in an NF-κB dependent manner. (A) Upper two panels: five micrograms of nuclear extracts prepared from B5 and h12 cells transduced with empty vector (EV2) or SR-IκBα (SR) were analyzed by EMSA, using NF-κB and Oct-1 probes. Middle 5 panels: whole-cell extracts (30 μg) of B5 or h12 infectants were subjected to SDS-PAGE and immunoblotting with anti-p52, anti-phospho-IκBα, anti-IκBα or anti-actin antibodies. Bottom panel: HA-tagged NIK was immunoprecipitated from B5 and h12 infectants with anti-HA antibody and detected by immunoblotting with anti-NIK antibody (H-248). (B) Phase-contrast micrographs of cells cultured on monolayers (upper images) or in soft

agar (lower images). B5 or h12 cell clones expressing wild type NIK (NIK#1 and NIK#2) or not (EV1) were cultured in soft agar for 3 weeks. These cells were further transduced with SR-IκBα, and then pooled cells were assayed for anchorage-independent growth in soft agar. B5 and h12 cell clones expressing kd-NIK were also examined. Original magnification: ×100. Abbreviations used: SR; super-repressor, kd-NIK; catalytically inactive NIK, IB; Immunoblotting, IP; Immunoprecipitation.

Figure 6. Depletion of NIK suppresses NF-κB-dependent transcription in ATL cells. (A) ED40515(-) and ATL-43Tb(-) cells were infected with lentiviral vectors expressing Renilla luciferase (Ctli) or NIK-specific shRNAs (NIKi-1 or NIKi-2). In parallel, ED40515(-) and ATL-43Tb(-) cells were infected with lentiviral vectors expressing Ctli or NIKi-1 shRNAs, and 24 hours later, these cells were super-infected with lentiviral vectors expressing Ctli or NIKi-2 shRNAs. Twenty-four hours after infection, cells were selected with puromycin for 2 days. Puromycin-resistant cells were then transfected with 2 μg of IgκCona-Luc and 2 μg EF1-LacZ. Luciferase (LUC) activity was determined 48 hours after transfection and normalized to β-gal activity. Relative luciferase activities, in comparison with control cells (100), are shown. Data are expressed as mean ± SD of three independent experiments. P values are versus control (Ctli). (B) Super-infected cells were treated with or without MG132 (20 μM) for 3 hours and subjected to SDS-PAGE and immunoblotting with either anti-NIK (#4994), anti-phosphorylated p100 or anti-α-tubulin antibodies. Whole-cell extracts (30 μg)

from these cells were analyzed by SDS-PAGE and immunoblotting with anti-phospho-IκBα, anti-IκBα or anti-α-tubulin antibodies. Cytoplasmic extracts prepared from ED40515(-) cells infected or not with lentivirus were precleared and immunoprecipitation was performed, using anti-IKK1 monolconal antibody or its isotype IgG (IgG). After 3 washes with TNT buffer, immune-complexes were treated or not with Shrimp Akaline Phosphatase (Takara Bio Inc.), and then subjected to SDS-PAGE and immunoblotting with anti-phospho-IKK1/2, anti-IKK1 or anti-IKK2 antibodies. (C) Five micrograms of nuclear extracts prepared from lentivirus-infected cells shown in (B) were analyzed by EMSA, using oligonucleotides encoding the NF-κB-binding sequence or Oct-1-binding sequence as probes. (D) Nuclear extracts (5 μg) from lentivirus-infected cells shown in (B) were pre-incubated for 30 minutes with purified mouse IgG, anti-p50, anti-cRel antibody, pre-immune (PI), anti-p50, anti-RelA or anti-RelB sera, and then subjected to EMSA with the NF-κB-specific probe. (E) Total RNAs from lentivirus-infected cells shown in (B) were examined by quantitative RT-PCR for *vegf*, *icam-1* and *mmp-9* mRNA levels. Each mRNA level was normalized to 18S RNA. Relative mRNA levels, in comparison with control cells (100), are shown. Data are expressed as mean ± SD of three independent experiments. P values are versus control (Ctli+Ctli).

Figure 7. Depletion of NIK in ATL cells suppresses tumor formation in NOD-SCID/γc^{null} (NOG) mice. (A) Pools of ED40515(-) cells expressing Ctli or NIKi-1 and -2 shown in Figure 6B, C, D and E were analyzed for cell growth *in vitro* by the

trypan blue staining method. Relative cell numbers, in comparison with control cells (arbitrarily set at 1), are shown. Data are expressed as mean ± SD of three independent experiments. P values are versus control (Ctli+Ctli). n.s. ; no significant difference. (B-D) NOG mice were inoculated subcutaneously in the post-auricular region with the puromycin-resistant ED-40515(-) cells (5×10^6). Tumor formation in mice was evaluated 2 weeks after inoculation. Tumor weight (B) and size (C) relative to those of tumors formed in mice inoculated with ED40515(-) cells expressing Ctli are shown. (D) Photographs of tumors formed 2 weeks after cell inoculation. Each result was obtained from five different mice (means are shown [error bars]). P values are versus control (Ctli+Ctli).

Figure 1

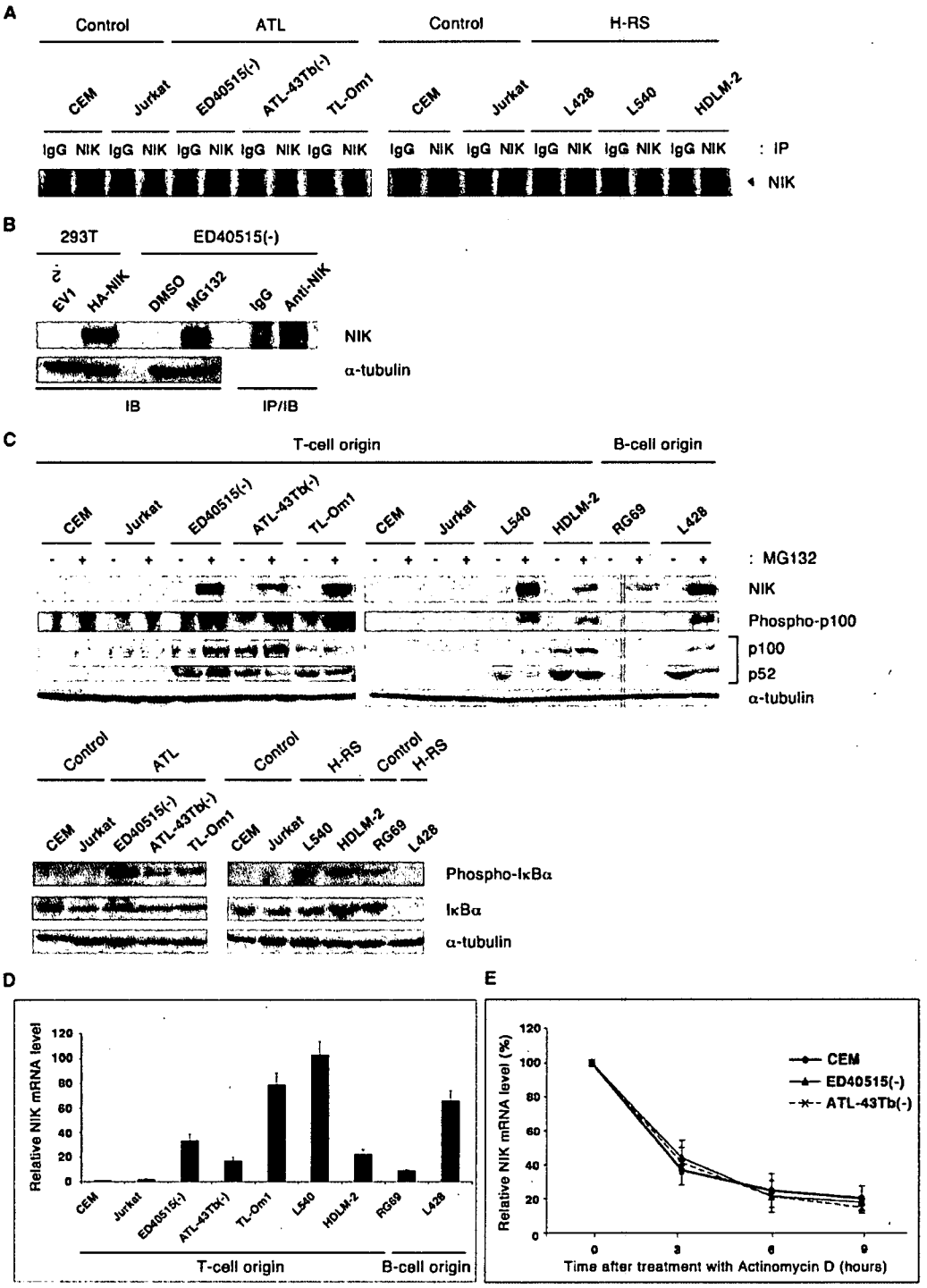
A
Control
ATL
Control
H-RS
CEM
Jurkat
ED40515(-)
ATL-43Tb(-)
TL-Om1
CEM
Jurkat
L428
L540
HDLM-2
IgG NIK IgG NIK IgG NIK IgG NIK IgG NIK IgG NIK IgG NIK IgG NIK IgG NIK IgG NIK
: IP
NIK
B
293T
ED40515(-)
EV1
HA-NIK
DMSO
MG132
IgG
Anti-NIK
NIK
α-tubulin
IB
IP/IB
C
T-cell origin
B-cell origin
CEM
Jurkat
ED40515(-)
ATL-43Tb(-)
TL-Om1
CEM
Jurkat
L540
HDLM-2
RG69
L428
: MG132
NIK
Phospho-p100
p100
p52
α-tubulin
Control
ATL
Control
H-RS
Control
H-RS
Phospho-IκBα
IκBα
α-tubulin
D
Relative NIK mRNA level
120
100
80
60
40
20
0
CEM
Jurkat
ED40515(-)
ATL-43Tb(-)
TL-Om1
L540
HDLM-2
RG69
L428
T-cell origin
B-cell origin
E
Relative NIK mRNA level (%)
120
100
80
60
40
20
0
CEM
ED40515(-)
ATL-43Tb(-)
0
3
6
9
Time after treatment with Actinomycin D (hours)

Figure 2

A

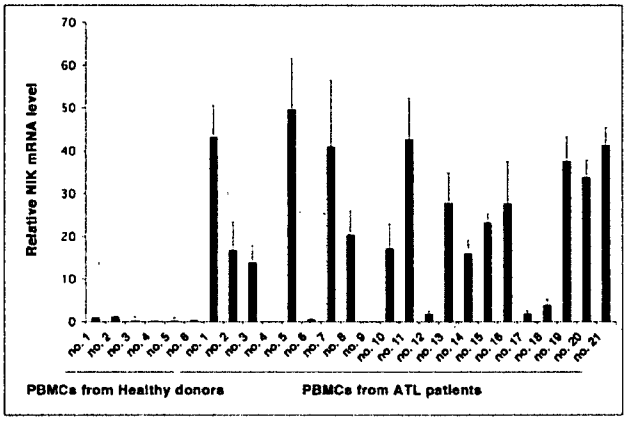
Relative NIK mRNA level
70
60
50
40
30
20
10
0
no. 1 no. 2 no. 3 no. 4 no. 5 no. 6 no. 1 no. 2 no. 3 no. 4 no. 5 no. 6 no. 7 no. 8 no. 9 no. 10 no. 11 no. 12 no. 13 no. 14 no. 15 no. 16 no. 17 no. 18 no. 19 no. 20 no. 21
PBMCs from Healthy donors
PBMCs from ATL patients

B

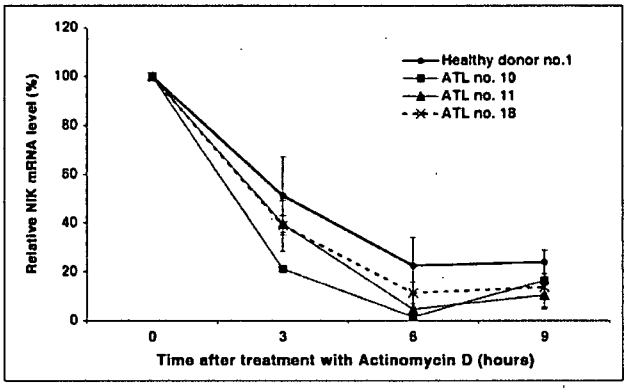
Relative NIK mRNA level (%)
120
100
80
60
40
20
0
Healthy donor no.1
ATL no. 10
ATL no. 11
ATL no. 18
0
3
6
9
Time after treatment with Actinomycin D (hours)

C

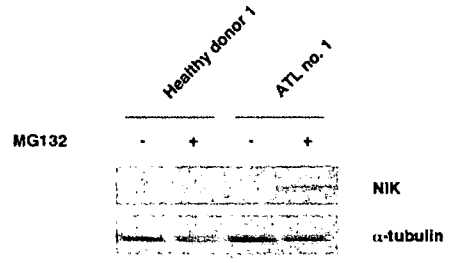
Healthy donor 1
ATL no. 1
MG132
- + - +
NIK
α-tubulin

Figure 3

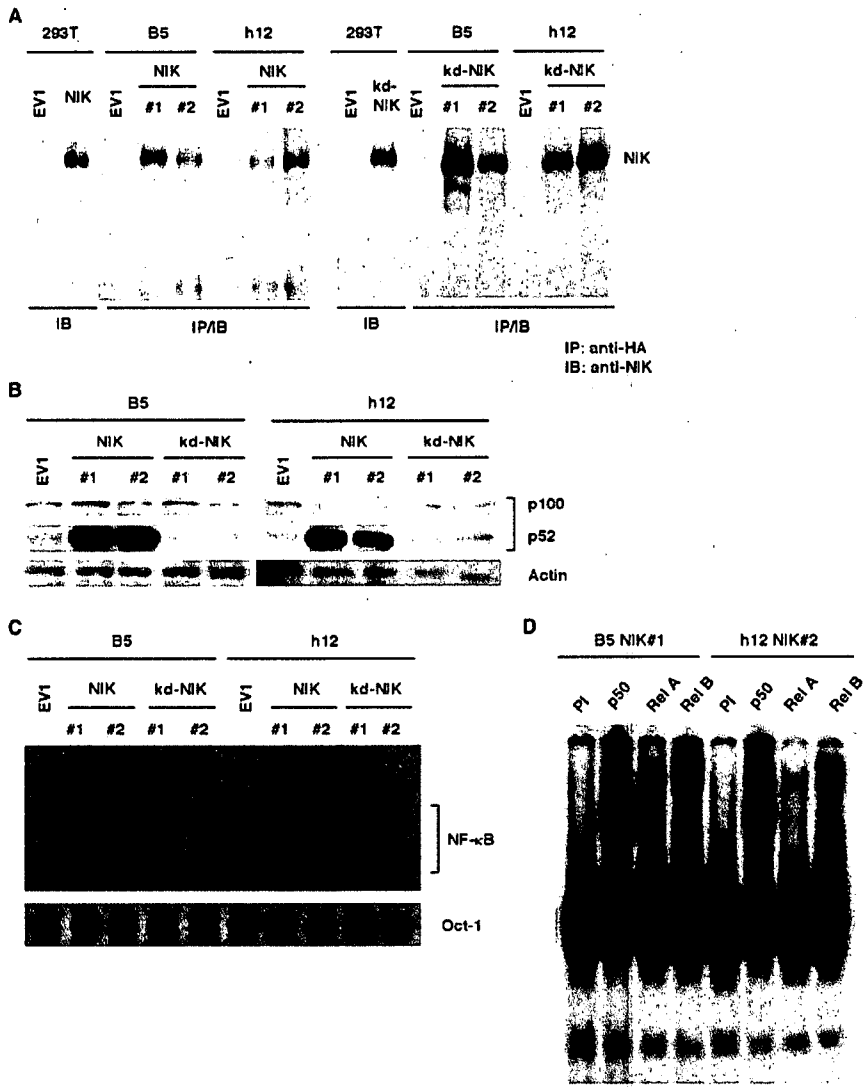
A
293T
B5
h12
293T
B5
h12
NIK
kd-NIK
EV1
NIK
#1
#2
kd-NIK
NIK
IB
IP/IB
IP: anti-HA
IB: anti-NIK
B
B5
h12
p100
p52
Actin
C
NF-κB
Oct-1
D
B5 NIK#1
h12 NIK#2
PI
p50
Rel A
Rel B

Figure 4

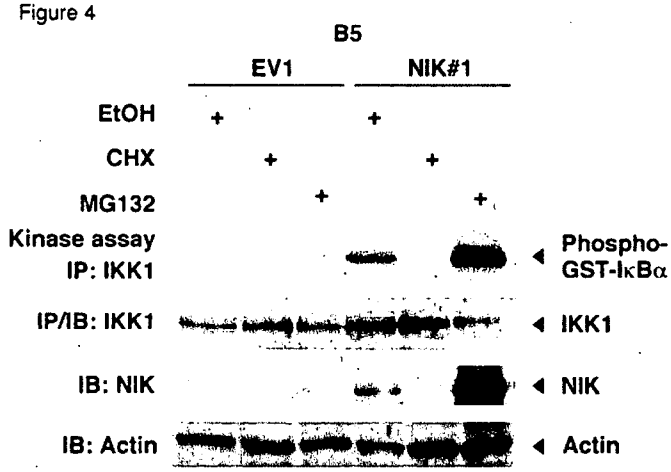
B5
EV1
NIK#1
EtOH
CHX
MG132
Kinase assay
IP: IKK1
Phospho-
GST-IκBα
IP/IB: IKK1
IKK1
IB: NIK
NIK
IB: Actin
Actin

Figure 5

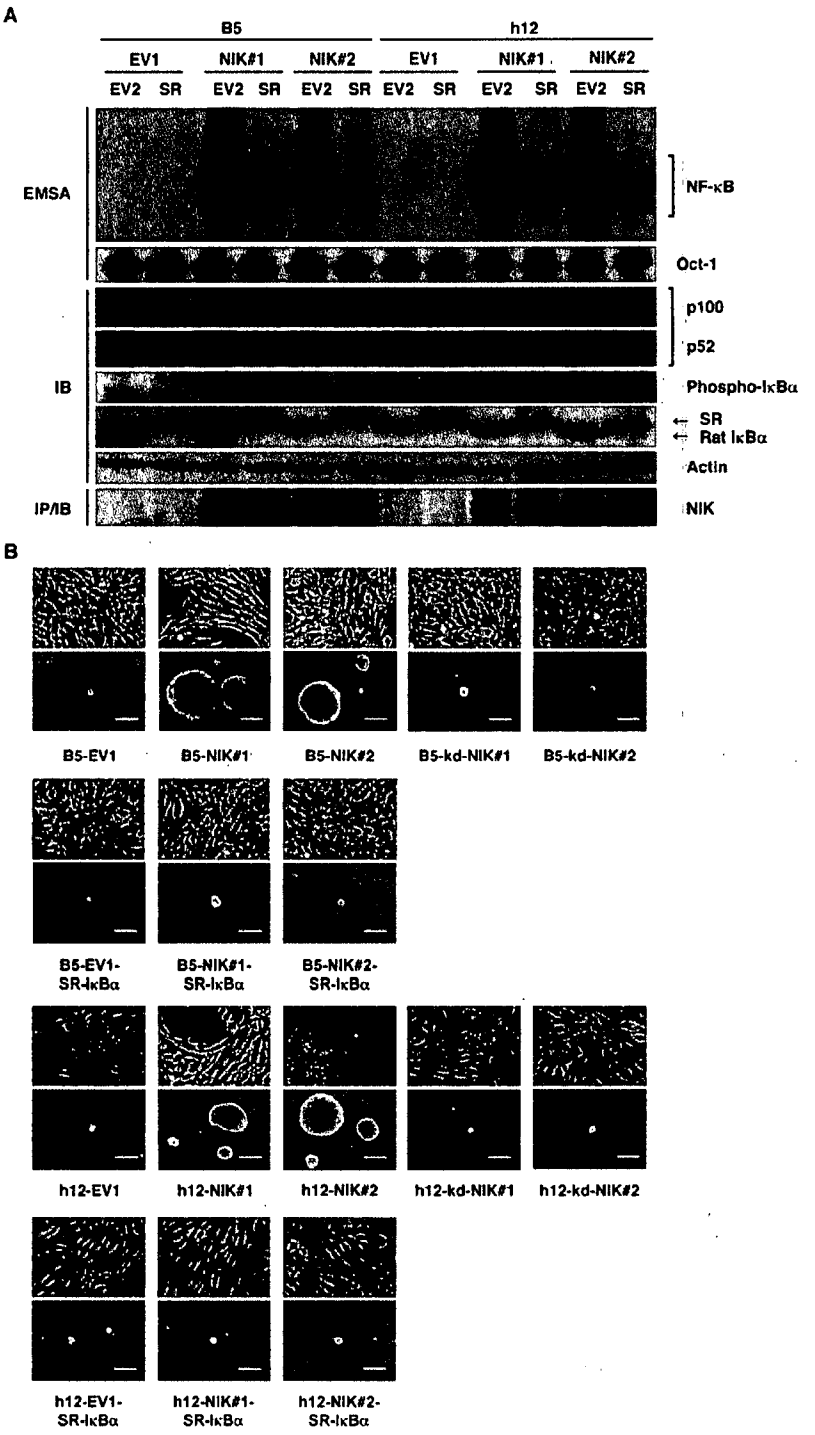
A
B5
h12
EV1
NIK#1
NIK#2
EV1
NIK#1
NIK#2
EV2 SR EV2 SR EV2 SR EV2 SR EV2 SR EV2 SR
EMSA
NF-κB
Oct-1
p100
p52
IB
Phospho-IκBα
SR
Rat IκBα
Actin
IP/IB
NIK
B
B5-EV1
B5-NIK#1
B5-NIK#2
B5-kd-NIK#1
B5-kd-NIK#2
B5-EV1-SR-IκBα
B5-NIK#1-SR-IκBα
B5-NIK#2-SR-IκBα
h12-EV1
h12-NIK#1
h12-NIK#2
h12-kd-NIK#1
h12-kd-NIK#2
h12-EV1-SR-IκBα
h12-NIK#1-SR-IκBα
h12-NIK#2-SR-IκBα

Figure 6

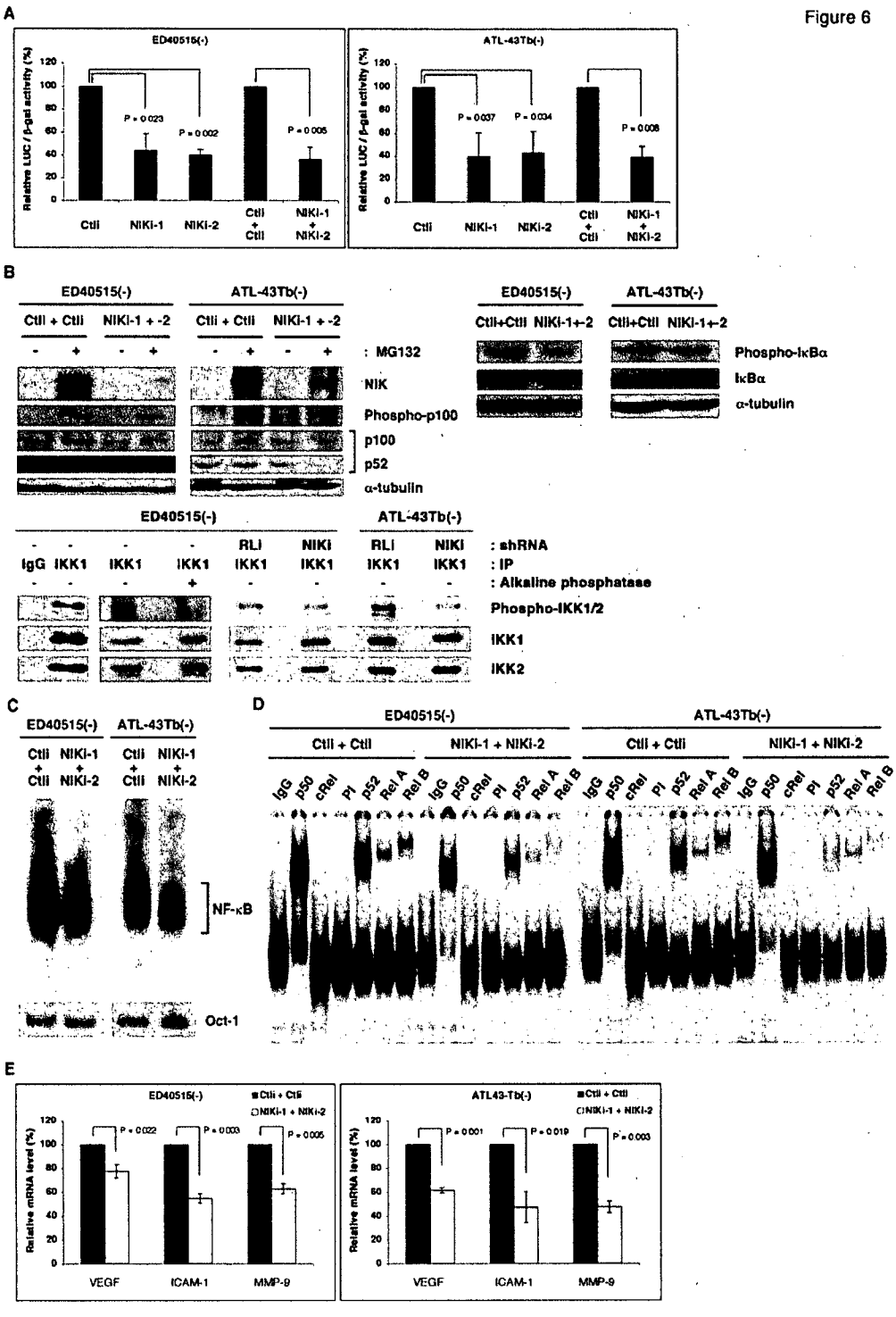
A
ED40515(-)
ATL-43Tb(-)
Relative LUC / β-gal activity (%)
P = 0.023
P = 0.002
P = 0.005
P = 0.037
P = 0.034
P = 0.008
Ctli
NIKi-1
NIKi-2
Ctli + Ctli
NIKi-1 + NIKi-2
B
ED40515(-)
ATL-43Tb(-)
Ctli + Ctli
NIKi-1 + -2
: MG132
NIK
Phospho-p100
p100
p52
α-tubulin
Phospho-IκBα
IκBα
α-tubulin
IgG
IKK1
RLI
NIKi
: shRNA
: IP
: Alkaline phosphatase
Phospho-IKK1/2
IKK1
IKK2
C
NF-κB
Oct-1
D
IgG
p50
cRel
PI
p52
Rel A
Rel B
E
Relative mRNA level (%)
P = 0.022
P = 0.003
P = 0.005
P = 0.001
P = 0.019
P = 0.003
VEGF
ICAM-1
MMP-9

Figure 7

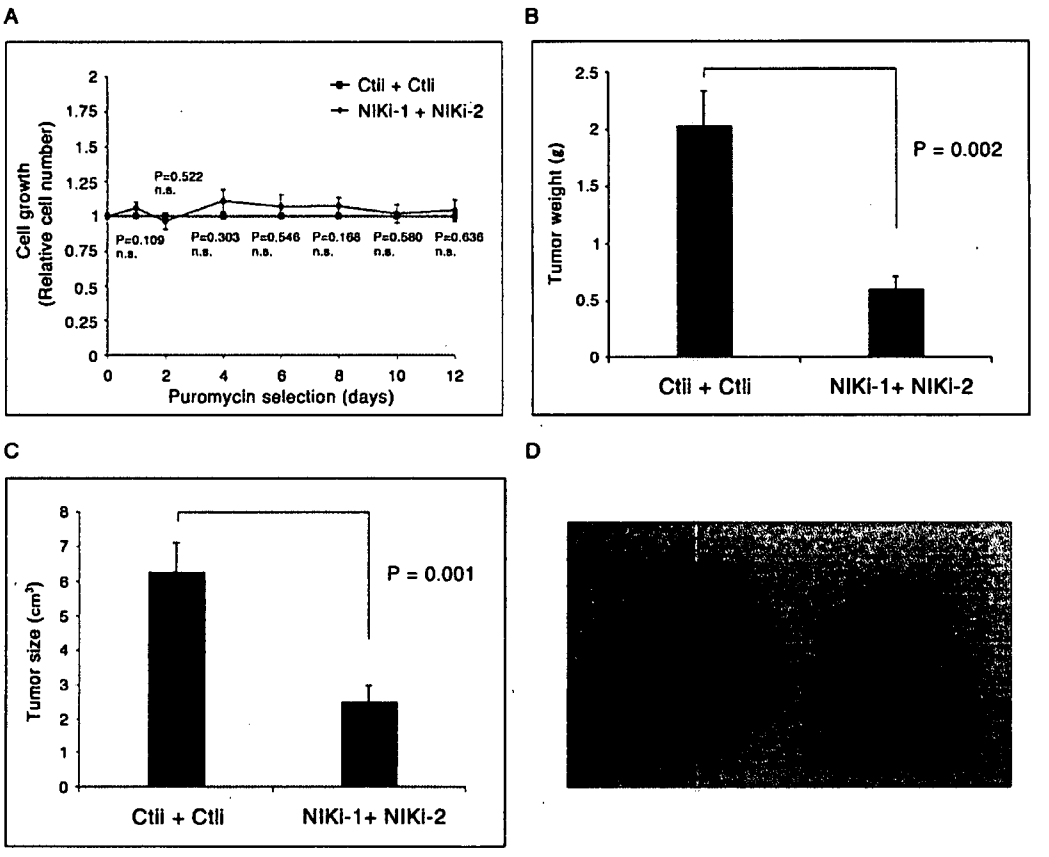
A
Ctli + Ctli
NIKi-1 + NIKi-2
Cell growth (Relative cell number)
Puromycin selection (days)
P=0.522 n.s.
P=0.109 n.s.
P=0.303 n.s.
P=0.546 n.s.
P=0.168 n.s.
P=0.580 n.s.
P=0.636 n.s.
B
Tumor weight (g)
P = 0.002
Ctli + Ctli
NIKi-1+ NIKi-2
C
Tumor size (cm³)
P = 0.001
Ctli + Ctli
NIKi-1+ NIKi-2
D

Molecular allelokaryotyping of pediatric acute lymphoblastic leukemias by high-resolution single nucleotide polymorphism oligonucleotide genomic microarray

Norihiko Kawamata,[1] Seishi Ogawa,[2] Martin Zimmermann,[3] Motohiro Kato,[2] Masashi Sanada,[2] Kari Hemminki,[4] Go Yamatomo,[2] Yasuhito Nannya,[2] Rolf Koehler,[5] Thomas Flohr,[5] Carl W. Miller,[1] Jochen Harbott,[6] Wolf-Dieter Ludwig,[7] Martin Stanulla,[3] Martin Schrappe,[8] Claus R. Bartram,[5] and H. Phillip Koeffler[1]

[1]Department of Hematology, Oncology, Cedars-Sinai Medical Center/University of California at Los Angeles School of Medicine; [2]Regeneration Medicine of Hematopoiesis, University of Tokyo, School of Medicine, Tokyo, Japan; [3]Department of Pediatric Hematology and Oncology, Children's Hospital, Hannover Medical School (MHH), Hannover, Germany; [4]Division of Molecular Genetic Epidemiology, German Cancer Research Center (DKFZ), Heidelberg, Germany; [5]Institute of Human Genetics, University of Heidelberg, Heidelberg, Germany; [6]Department of Pediatric Hematology and Oncology, Justus Liebig University, Gießen, Germany; [7]Department of Hematology, Oncology and Tumor Immunology, Robert-Rössle-Clinic at the HELIOS-Clinic Berlin-Buch, Charité, Berlin, Germany; and [8]Department of Pediatrics, University of Kiel, Kiel, Germany

Pediatric acute lymphoblastic leukemia (ALL) is a malignant disease resulting from accumulation of genetic alterations. A robust technology, single nucleotide polymorphism oligonucleotide genomic microarray (SNP-chip) in concert with bioinformatics offers the opportunity to discover the genetic lesions associated with ALL. We examined 399 pediatric ALL samples and their matched remission marrows at 50 000/250 000 SNP sites using an SNP-chip platform. Correlations between genetic abnormalities and clinical features were examined. Three common genetic alterations were found: deletion of *ETV6*, deletion of *p16INK4A*, and hyperdiploidy, as well as a number of novel recurrent genetic alterations. Uniparental disomy (UPD) was a frequent event, especially affecting chromosome 9. A cohort of children with hyperdiploid ALL without gain of chromosomes 17 and 18 had a poor prognosis. Molecular allelokaryotyping is a robust tool to define small genetic abnormalities including UPD, which is usually overlooked by standard methods. This technique was able to detect subgroups with a poor prognosis based on their genetic status. (Blood. 2008;111:776-784)

Introduction

Pediatric acute lymphoblastic leukemia (ALL) is the most common malignant disease in children.[1-3] ALL is a genetic disease resulting from accumulation of mutations of tumor suppressor genes and oncogenes.[1-3] Knowledge of these mutations can be of use for diagnosis, prognosis, and therapeutic clinical purposes, as well as to provide an overall understanding of the pathogenesis of ALL.[1-3] Identification of mutated genes in ALL has evolved with improvement in technology. A recent approach is single nucleotide polymorphism (SNP) analysis using an array-based technology[4,5] that allows identification of amplifications, deletions, and allelic imbalance, such as uniparental disomy (UPD [represents the doubling of the abnormal allele due to somatic recombination or duplication and loss of the other normal allele]).[6-8] However, since this technique detects allelic dosage, it cannot detect balanced translocations.

According to the HapMap publication, 9.2 million SNPs have been reported, and of these, 3.6 million have been validated.[9] Global genomic distribution of SNPs and its easy adaptability for high throughput analysis make them the target of choice to look for genomic abnormalities in ALL and other cancers.[5-7]

Recently, higher resolution SNP-chip (50 000-500 000 probes) has been developed for large-scale SNP typing.[4,10] With a large number of SNP probes, in combination with the algorithms specifically developed for copy number calculations, these SNP-chips enable genomewide detection of copy number changes.[11,12] The combination of SNP-chip technology, nucleotide sequencing, and bioinformatics allows the investigator to view the entire genome of ALL in an unbiased, comprehensive approach. Using SNP-chips, the chromosomal abnormalities can be evaluated at a very high resolution (molecular level: average distances of each probe are 47 kb and 5.8 kb in the 50 k/500 k arrays, respectively[4,10]), and allele-specific gene dosage level (gene dosage of paternal and maternal alleles) also can be analyzed in the whole genome.[11,12] Hence, we name this new technology "molecular allelokaryotyping."[12] In this study, we performed molecular allelokaryotyping on a very large cohort (399) of pediatric ALL samples to examine genomic abnormalities at high resolution. Further, we examined correlations between the genomic abnormalities detected by SNP-chip and clinical features, including prognosis.

Submitted May 1, 2007; accepted September 13, 2007. Prepublished online as *Blood* First Edition paper, September 21, 2007; DOI 10.1182/blood-2007-05-088310.

N.K., S.O., and M.Z. equally contributed to this work as first authors. C.R.B. and H.P.K. equally contributed to this work as last authors.

An Inside *Blood* analysis of this article appears at the front of this issue.

The online version of this article contains a data supplement.

The publication costs of this article were defrayed in part by page charge payment. Therefore, and solely to indicate this fact, this article is hereby marked "advertisement" in accordance with 18 USC section 1734.

Methods

Clinical samples and DNA/RNA preparation

The ALL-BFM 2000 trial of the Berlin-Frankfurt-Münster (BFM) study group on treatment of childhood ALL enrolled patients from ages 1 year to 18 years at diagnosis.

From September 1999 to January 2002, 566 patients were consecutively enrolled in this trial. The ALL-BFM 2000 study was approved by the ethics committees of the Medical School Hanover and the Cedar Sinai Medical Center. Informed consent was obtained in accordance with the Declaration of Helsinki.

Of the 566 patients (nos. 299-854), 399 patients, representing 70% of the entire patient population, had additional DNA available and could be included in the present SNP-chip study. The 167 patients not available for this analysis did not differ from the 399 patients in this study with regard to their clinical and biological characteristics (data not shown).

Complete remission (CR) was defined as the absence of leukemia blasts in the peripheral blood and cerebrospinal fluid, fewer than 5% lymphoblasts in marrow aspiration smears, and no evidence of localized disease. At day 29, bone marrows were examined, and all patients in this SNP-chip analysis study obtained a CR at that time. The remission marrows were collected and used as matched control for the SNP-chip analysis.

Prednisone response was defined based on numbers of peripheral blood blasts per microliter on day 8, and patients were classified into good (< 1000 blasts/μL) and poor responders (≥ 1000 blasts/μL).[13-15] Relapse was defined as recurrence of lymphoblasts or localized leukemic infiltrates at any site.

DNA index, immunophenotyping, molecular analysis of chromosomal abnormalities

Leukemic or normal bone marrow cells were stained with propidium iodide, and cellular DNA contents were measured by cytometric analysis as previously reported.[16,17] DNA index was defined as the DNA content of leukemic cells compared with normal G0/G1 cells. When the DNA index of leukemic cells was the same as or greater than 1.16, it was defined as hyperdiploid ALL by DNA index as previously reported.[16,17]

Immunophenotyping of ALL was examined using anti-CD2, -CD3, -CD4, -CD10, -CD19, and -CD20 antibodies by FACS.[13-15] ETV6/RUNX1, BCR/ABL, and MLL/AF4 were examined by interphase fluorescence in situ hybridization (FISH) analysis using specific probes and by reverse transcriptase–polymerase chain reaction (RT-PCR) using specific primers for these fusion transcripts as described previously.[13-15]

Molecular allelokaryotyping of leukemic cells

DNA from the 399 ALL samples as well as their paired normal DNA from remission samples were analyzed on Affymetrix GeneChip human mapping 50 K *Xba*I or 250 K Nsp arrays (Affymetrix Japan, Tokyo, Japan) according to the manufacturer's protocol. Microarray data were analyzed for determination of both total and allelic-specific copy numbers using the CNAG program as previously described[11,12] with minor modifications, where the status of copy numbers as well as UPD at each SNP was inferred using the algorithms based on Hidden Markov Models.[11,12]

For clustering of ALL samples with regard to the status of copy number changes as well as UPD, entire genome was divided into contiguous sub-blocks of 100 kb in length, and according to the inferred copy numbers (CNs) and the status of UPD, one of the 4 conditions was assigned to the *i*th sub-block (*Si*); CN gain, CN loss, normal CN, and UPD. For a given 2-copy number data, A and B, distance (d[A,B]) was simply defined as

$$d(A,B) = \sum_i I(S_i^A; S_i^B)$$

$$I(S_i^A; S_i^B) = \begin{cases} 1 \text{ if } S_i^A = S_i^B \\ 0 \text{ if } S_i^A \neq S_i^B \end{cases}$$

where S_i^A and S_i^B are the status of the *i*th sub-block (*Si*) in data A and B, respectively, and sum is taken for all sub-blocks. Clustering was initiated by finding a seed cluster of 2 samples showing the minimum distance and replacing them with the cluster data having the mean *Si* value of the two. This procedure was iteratively performed until all samples were converged to one cluster based on this distance using a program developed for this purpose (GNAGraph), which was followed by manual revisions focusing on particular genetic lesions selected by their frequencies within the sample set. CNAG and CNAGraph are available on request.

Quantitative genomic PCR and direct sequencing

Quantitative genomic PCR (qPCR) was performed on a real-time PCR machine, iCycler (Bio-Rad Laboratories, Hercules, CA) using iQ cybergreen supermix (Bio-Rad Laboratories) according to the manufacturer's protocol. Primer sequences used for the qPCR are listed in Table S2 (available on the *Blood* website; see the Supplemental Materials link at the top of the online article). Gene dosage at the 2p allele was used as an internal control. Allelic gene dosage of 9p and 9q was measured, and these were compared with the levels in respective matched control DNA. SNP sites were amplified and directly sequenced on Autosequencer 3000 (Applied Biosystems, Foster City, CA). Primers used for SNP site amplification are listed in Table S2. Exons 12 and 14 of JAK2 gene were amplified as previously reported.[18] PCR products were purified and subjected to direct sequencing.

Data preparation

Proportional differences between groups were analyzed by either chi-squared (χ^2) or Fisher exact tests. The Kaplan-Meier method was used to

Table 1. Characterization of clinical features of 399 ALL cases

	Cases, no. (%)
Sex	
Male	230 (57)
Female	169 (43)
Age	
1 to 9 yrs	307 (77)
Older than 10 yrs	92 (23)
WBC	
Below $10^2 \times 10^9$/L	362 (91)
Over $10^2 \times 10^9$/L	37 (9)
Immunophenotype	
T-cell	49 (12)
B-cell	339 (85)
Unknown	11 (3)
CNS involvement	
Yes	11 (3)
No	358 (90)
unknown	30 (7)
BCR/ABL	
Yes	6 (2)
No	379 (95)
Unknown	14 (3)
ETV6/RUNX1	
Yes	96 (24)
No	270 (68)
Unknown	33 (8)
PDN response	
Good	360 (90)
Poor	35 (9)
Unknown	4 (1)

WBC indicates white blood cell count (× 10^9/L) in peripheral blood at diagnosis; CNS involvement, central nervous system involvement at diagnosis; *BCR/ABL* and *ETV6/RUNX1*, *BCR/ABL* or *ETV6/RUNX1* fusion was examined by RT-PCR and/or FISH analysis; PDN, prednisone; and PDN response, blast cell count was 1000/μL or greater in peripheral blood after a 7-day exposure to prednisone and one intrathecal dose of methotrexate.